Published in final edited form as:

Cancer Res. 2022 December 02; 82(23): 4386–4399. doi:10.1158/0008-5472.CAN-22-1744.

Stress-mediated attenuation of translation undermines T-cell activity in cancer

Brian P. Riesenberg[1], **Elizabeth G. Hunt**[1,2], **Megan D. Tennant**[3], **Katie E. Hurst**[1], **Alex M. Andrews**[4], **Lee R. Leddy**[4], **David M. Neskey**[4], **Elizabeth G. Hill**[4,5], **Guillermo O. Rangel Rivera**[3,6], **Chrystal M. Paulos**[3,6], **Peng Gao**[7], **Jessica E. Thaxton**[1,2,#]

[1]Immunotherapy Program, Lineberger Comprehensive Cancer Center, University of North Carolina at Chapel Hill; Chapel Hill, NC 27514; USA

[2]Department of Cell Biology & Physiology, University of North Carolina at Chapel Hill; Chapel Hill, NC 27514; USA

[3]Department of Microbiology & Immunology, Medical University of South Carolina, Charleston, SC 29425; USA

[4]Hollings Cancer Center, Medical University of South Carolina, Charleston, SC 29425; USA

[5]Department of Public Health Sciences, Hollings Cancer Center Biostatistics Shared Resource; Director, Medical University of South Carolina, Charleston, SC 29425; USA

[6]Department of Surgery and Microbiology & Immunology, Winship Cancer Institute, Emory University, Atlanta, GA, 30322; USA

[7]Department of Medicine, Metabolomics Core Facility; Director, Feinberg School of Medicine, Northwestern University, Chicago, IL 60611; USA

Abstract

Protein synthesis supports robust immune responses. Nutrient competition and global cell stressors in the tumor microenvironment (TME) may impact protein translation in T cells and antitumor immunity. Using human and mouse tumors, we demonstrated here that protein translation in T cells is repressed in solid tumors. Reduced glucose availability to T cells in the TME led to activation of the unfolded protein response (UPR) element eIF2α. Genetic mouse models revealed that translation attenuation mediated by activated p-eIF2α undermines the ability of T cells to suppress tumor growth. Reprogramming T cell metabolism was able to alleviate p-eIF2α accumulation and translational attenuation in the TME, allowing for sustained protein translation. Metabolic and pharmacological approaches showed that proteasome activity mitigates induction of p-eIF2α to support optimal antitumor T cell function, protecting from translation attenuation and enabling prolonged cytokine synthesis in solid tumors. Together, these data identify a new therapeutic avenue to fuel the efficacy of tumor immunotherapy.

[#]Correspondence: Dr. Jessica Thaxton, Department of Cell Biology & Physiology, Immunotherapy Program, Lineberger Comprehensive Cancer Center, University of North Carolina at Chapel Hill, 125 Mason Farm Road, Chapel Hill, NC 27514, 919-966-4913, jess_thaxton@med.unc.edu.

Conflict of Interest:
The authors declare no potential conflicts of interest.

Keywords

T cell; immunotherapy; tumor immunology; metabolism; protein synthesis; catabolism; proteasome; glucose

Introduction

Activation of protein synthesis is a requirement for T cell growth and effector function (1). Eukaryotic translation initiation factor 2 (eIF2) controls cap-dependent protein translation efficiency by bridging Met-tRNA$_i$ and the ribosomal subunit (2). However, endoplasmic reticulum (ER) stress, catalyzed by accrual of unfolded proteins in the ER lumen, undermines the competency of the process. In response to ER stress, the unfolded protein response (UPR) is initiated via phosphorylation of the α subunit of eIF2 causing translation attenuation as a means to restore proteostasis (3). The tumor microenvironment (TME) is replete with metabolic stressors known to activate the UPR (4-7). We and others have shown that PKR-ER-like kinase (PERK), a stress sensor responsible for eIF2α phosphorylation (8,9), undermines T cell antitumor efficacy (10,11). While these studies implicate the UPR-mediated translational machinery as a potential molecular checkpoint prompted by TME stress, the extent to which translational regulation influences outcomes in the context of antitumor immunity is unknown.

Glycolysis is the critical energy requirement for T cells to undergo protein translation (12). However, upon entering the TME CD8 T cells encounter competition for exogenous glucose resulting in a significant reduction in effector function (5). In contrast, T cells that depend on metabolic pathways apt for cell survival in nutrient stress, such as gluconeogenesis (13) or fatty acid oxidation (14), demonstrate heightened tumor control (15,16). Metabolic reprogramming through cytokine conditioning (17) or chronic glucose deprivation (15) generates T cells enriched for such pathways that fuel sustenance in nutrient deplete settings. While we previously demonstrated that metabolic reprogramming through cytokine conditioning generates T cells capable of sustaining protein translation in solid tumors (18), the underlying mechanism supporting this phenomenon remains unknown.

The proteasome is a proteolytic complex responsible for the degradation of ubiquitinated proteins (19). Proteasome inhibition exacerbates ER stress and promotes the UPR, rendering tumor cells susceptible to apoptosis (20). The relationship between protein translation and degradation is symbiotic, as effective protein catabolism precludes activation of the UPR. Memory T cells, the T cell subset with heightened antitumor efficacy, are enriched for proteasome subunits and exhibit accelerated protein degradation (21). Activation of the proteasome promotes memory T cell lineage development, linking protein degradation to memory fate (22). Indeed, memory like T cells are capable of sustaining protein synthesis under TME stress; however, the synergy between sustained translation, protein degradation, mitigating the UPR, and optimal antitumor immunity has not been studied.

In the present study we investigated the contribution of stress-mediated attenuation of translation to inhibit antitumor T cell efficacy. We found that the TME induces eIF2α phosphorylation, driven by nutrient deprivation, to restrict protein synthesis and tumor

control in T cells. Metabolic reprograming was able to alleviate accumulation p-eIF2α, promoting continued translation in the TME. Sustained protein synthesis was dependent on robust proteasome activation, protecting T cells from p-eIF2α mediated translation attenuation, proving critical for tumor control. These data indicate that protein degradation underlies antitumor metabolism and translation that can be harnessed to amplify T cell tumor immunity.

Materials and Methods

Human samples

Patients undergoing surgical removal of tumors granted written informed consent via MUSC Biorepository surgical consent forms. All study participants had not recently undergone chemo or irradiation therapy. This work was determined by MUSC Institutional Review Board to be exempt under protocol Pro00050181. Tissue samples were de-identified. Studies were conducted in accordance with the Declaration of Helsinki, International Ethical Guidelines for Biomedical Research Involving Human Subjects (CIOMS), Belmont Report, or U.S. Common Rule. Blood (8 mL) was collected in EDTA-coated tubes and PBMCs were isolated via Histopaque-1077 centrifugation. Tumor tissue was collected on ice, cut into 2-mm^3 pieces then dissociated to single-cell suspensions using the human tumor dissociation kit and gentleMACS dissociator (Miltenyi Biotech) according to the manufacturer's protocol. For normal human donor experiments, PBMCs and ImmunoCult Human CD3/CD28 T cell activators were obtained from Stemcell Technologies (RRID: AB_2827806).

Mice

OT-1 (C57BL/6-Tg(TcraTcrb)1100Mjb/J, RRID: IMSR_JAX:003831), $eIF2\alpha^{S51A+/-}$ (B6;129-Eif2s1^{tm1Rjk}/J, RRID: IMSR_JAX:017601), $PERK^{f/f}$ (*Eif2ak3*$^{tm1.2Drc}$/J), LCK-*cre* (B6.Cg-Tg(Lck-icre)3779Nik/J, RRID: IMSR_JAX:012837), CD45.1 (B6.SJL-*Ptprc*^{a} *Pepc*^{b}/BoyJ, RRID: IMSR_JAX:002014), pmel (B6.Cg-*Thy1*^{a}/Cy Tg(TcraTcrb)8Rest/J, RRID: IMSR_JAX:005023) and C57BL/6J (RRID: IMSR_JAX:000664) mice were obtained from the Jackson Laboratory. All animal experiments were approved by both the Medical University of South Carolina (MUSC) Institutional Animal Care and Use Committee and the University of North Carolina at Chapel hill (UNC) Division of Comparative Medicine. Mice were maintained by the Division of Laboratory Animal Resources at MUSC and Division of Comparative Medicine at UNC.

Cell cultures

B16F1 (ATCC, RRID: CVCL_0158), B16F1-OVA (Kind gift of Dr. Mark Rubinstein), and MCA-205 (Millipore-Sigma, RRID: CVCL_VR90) tumor lines and OT-1 T cells were maintained in RPMI supplemented with 10% FBS, 300 mg/L L-glutamine, 100 units/mL penicillin, 100 μg/mL streptomycin, 1mM sodium pyruvate, 100μM NEAA, 1mM HEPES, 55μM 2-mercaptoethanol, and 0.2% Plasmocin mycoplasma prophylactic. 0.8 mg/mL Geneticin selective antibiotic was added to media of B16F1-OVA cells for multiple passages then cells were passaged once in the Geneticin-free media prior to tumor implantation. MC-38 (Kerafast, RRID: CVCL_B288) and 293-T cells (ATCC, RRID: CVCL_0063)

were maintained in DMEM supplemented with 10% FBS, 100 units/mL penicillin, 100 μg/mL streptomycin, and 0.2% Plasmocin mycoplasma prophylactic. All tumor lines were determined to be mycoplasma-free in May 2021. For OT-1 T cell activation and expansion, whole splenocytes from OT-1 mice were activated with 1 μg/mL OVA 257-264 peptide and expanded for 3 days with 200 U/mL rhIL-2 (NCI). In some experiments, T cells were split on day 3 and expanded in rhIL-2, IL-15 (50ng/mL), or Cyclosporine A (2.5μM) through day 7, or split to normal or low glucose (1mM) for 16 hours. Human PBMCs were activated with Immunocult™ CD3/CD28 T cell activators (STEMCELL Technologies, anti-human CD3 and anti-human CD28 monospecific antibody complexes) and expanded in 500U rhIL-2 (NCI), and cultures were maintained in RPMI supplemented with 10% FBS, 300 mg/L L-glutamine, 2mM GlutaMAX, 100 units/mL penicillin, 100 μg/mL streptomycin, 50 μg/mL gentamycin, 25mM HEPES, 55μM 2-mercaptoethanol, and 0.2% Plasmocin mycoplasma prophylactic.

Tumor models

For endogenous TIL analysis, B16F1 were established by injecting 2.5×10^5 cells subcutaneously into the right flank of female C57BL/6 mice. Tumor-draining lymph nodes, spleens, and tumors were harvested after 6 days of tumor growth for measurement of protein synthesis and cytokine production. For adoptive cellular therapy experiments, B16F1-OVA melanomas were established subcutaneously by injecting 2.5×10^5 cells into the right flank of female C57BL/6 mice and tumor-bearing hosts were irradiated with 5 Gy 24 hours prior to T cell transfer. After 7 days of tumor growth, 5×10^5 OT-1 WT, PERK KO, or $eIF2\alpha^{S51A+/-}$ T cells conditioned with IL2, IL15, vehicle, or Cyclosporin A were infused in 100 μL phosphate-buffered saline via tail vein into mice. For proteasome inhibition, vehicle or MG132 was added to T cells 4 hours prior to infusion. For adoptive cell therapy tumor harvest experiments, $1x10^6$ $CD45.2^+$ OT-1 or $Thy1.1^+$ pmel T cells treated with vehicle or Cyclosporine A were infused into C57BL/6 $CD45.1^+$ mice bearing B16-F1-OVA tumors or C57BL/6 mice bearing B16-F1 tumors, respectively. Tumors were harvested 5 days after T cell infusion using the mouse tumor dissociation kit gentleMACS dissociator (Miltenyi Biotech) according to the manufacturer's protocol. Tumor growth was measured every other day with calipers, and survival was monitored with an experimental endpoint of tumor growth ≥ 300 mm^2.

Tumor-T cell transwell assays and glucose measurement

$2x10^4$, $5x10^4$, $1x10^5$, $2x10^5$, or $4x10^5$ B16F1, MC-38, or MCA-205 tumor cells or 293-T human embryonic kidney cells were seeded into 6 or 12 well companion plates. After 24 hours, OT-1 T cells or PBMCs were introduced into Transwells inserts in complete T-cell media supplemented with 200 U rhIL-2 (NCI) or IL-15 (50ng/mL) and harvested 36 hours later. Mouse T cells were added to Transwells at peptide activation, and in other instances added after 3 days of expansion in 200 U/mL rhIL-2 (NCI). Human T cells were added to Transwells at soluble CD3/28 activation, and in other instances added after 1 week of expansion. For metabolic remodeling, high glucose (25mM), 2DG (1mM, chronic), IL-15 (50nM), or Cyclosporine A (2.5μM) were introduced at the time of T cell addition to transwells. For acute treatment, 2DG (1mM, acute), or MG132 (5μM) were added 2 and 4 hours prior to bioenergetic analysis, respectively. Glucose concentration in transwell assay

media with increasing tumor density was determined using the B61000 Blood Glucose System on the day of transwell assay harvest.

Immunoblotting

T cells were lysed in RIPA Buffer (Sigma) supplemented with Protease Inhibitor Cocktail (Cell Signaling Technology) and Phosphatase Inhibitors I and II (Sigma). Protein concentrations were normalized using Pierce BCA Kit (Thermo Fisher Scientific) and loaded to 4%–10% agarose gels (Bio-Rad). P-eIF2α, eIF2α, PERK, CHOP, ATF4, β-actin, and HRP-linked anti-rabbit and mouse secondaries were obtained from Cell Signaling Technology, ERO1α was obtained from Santa Cruz Biotechnologies. Phospho protein was developed with Pierce ECL Plus Western Blotting Substrate (Thermo Fisher Scientific).

Protein synthesis and flow cytometry

Homopropargylglycine (HPG) protein synthesis was measured using the Click-iT HPG Alexa Fluor 488 Protein Synthesis Assay Kit from Thermo Fisher Scientific. Cells were incubated in methionine-free media and controls were treated with cycloheximide. Cells were stained extracellularly using CD8-Alexa Fluor 647 (Biolegend, RRID:AB_389326) and subsequently incubated in 50μM L-HPG with added Live-or-Dye Fixable Viability Stain. Cells were fixed using Fixation Buffer (Biolegend) and permeabilized with Triton X-100 solution followed by staining with Alexa Fluor 488 Azide to label active protein synthesis. OPP protein synthesis was measured using the O-Propargyl-puromycin (OPP) Protein Synthesis Assay Kit (Cayman Chemical). T cells were incubated in complete T cell media, and control cells were treated with CHX. Cells were incubated in cell-permeable OPP, and Live-or-Dye Fixable Viability Stain was added. Cells were fixed using formaldehyde and subsequently stained with 5 FAM-Azide to label translating polypeptide chains. Cells were stained extracellularly using CD8-Alexa Fluor 647. Samples were run directly on a BD Accuri C6 flow cytometer and analysis was performed with FlowJo software (BD Biosciences, RRID: SCR_008520). For measurements of protein translation rates, each T cell condition was treated ± CHX, and CHX-treated wells were used to normalize protein synthesis rates in various *in vivo* and *in vitro* conditions defined as $\log_2$(T cell protein synthesis rate/T cell protein synthesis rate in the presence of CHX).

For proteasome activity analysis, Proteasome Activity Probe (R&D Systems) was stained on cells of interest at 2.5μM for 2 hours at 37 C in PBS. Samples were run directly on a BD Accuri C6 flow cytometer. For *in vitro* T cell phenotyping of vehicle, acute, or chronic 2DG treated, WT or eIF2α$^{S51A+/-}$, and vehicle or Cyclosporine A treated OT-1 or pmel T cells, samples were stained with Zombie NIR viability dye (Biolegend) in PBS at 4C for 15 minutes. After wash, cells were stained with a varied combination of CD8-Spark Blue 550 (Biolegend, RRID: AB_2819773), CD8-spark NIR 685 (Biolegend, RRID: AB_2819775), CD44-Brilliant Violet 785 (Biolegend, RRID: AB_2571953), CD62L-BV421 (BD Biosciences, RRID: AB_2737885), PD-1-BB700 (BD Biosciences, RRID: AB_2869777), TIM-3-Brilliant Violet 711 (Biolegend, RRID: AB_2716208), LAG-3-APC-eFluor 780 (Invitrogen, RRID:AB_2637323), ICOS-Super Bright 436 (Invitrogen, RRID: AB_2744818), CD69-PE/Cyanine5 (Biolegend, RRID: AB_313113), CD95-BV480 (BD Biosciences, RRID:AB_2744016), GITR-BV650 (BD

Biosciences, RRID:AB_2740316), CD27-BV750 (BD Biosciences, RRID:AB_2872091) for 30 minutes at 4C. Cells were washed and fixed overnight with using the Foxp3/Transcription Factor Fixation/Permeabilization Concentrate and Diluent kit and Permeabilization Buffer (eBioscience). Cells were then washed with 1x permeabilization buffer and stained with CTLA-4-PE-Dazzle 594 (Biolegend, RRID:AB_2564496), Ki67-PerCP-eFluor 710 (Invitrogen, RRID:AB_11040981), TOX-PE (Miltenyi Biotec,), TCF1/7-PE-Cy7 (Cell Signaling Technology), Granzyme B-Alexa Fluor 700 (Biolegend, RRID:AB_2728389), BCL-2-Alexa Fluor 647 (Biolegend, RRID:AB_2274702) for 3 hours at room temperature. Samples were collected on a Cytek Northern Lights and analyzed via Cytek SpectraFlo software.

Cytokine synthesis

For cytokine restimulated human and mouse T cells, in some instances cells grown in normal media or tumor supernatant were treated with cycloheximide for 30 minutes prior to being restimulated for 4 hours with Cell Stimulation Cocktail and GolgiPlug Brefeldin A (eBioscience). For tumor infiltrating T cell analysis, single cell suspensions were counted and plated at $5x10^5$ cells per well and stimulated with Cell Stimulation Cocktail and GolgiPlug Brefeldin A for 3 hours at 37C. Samples were then stained with Zombie NIR viability dye (Biolegend) followed CD45.2-BV510 (Biolegend, RRID:AB_2561393) and CD8-Alexa Fluor 647. IFNγ-PE (Invitrogen, RRID:AB_466192) and TNF-α-FITC (Invitrogen, RRID:AB_465418) intracellular FACS staining was performed using the Foxp3/Transcription Factor Fixation/Permeabilization Concentrate and Diluent kit and Permeabilization Buffer (eBioscience). Samples were run on a BD Accuri C6 flow cytometer or a Cytek Northern Lights and analysis was performed with FlowJo software.

Seahorse bioanalysis

Seahorse XF Real-Time ATP Rate assays were performed using the Seahorse XFe96 analyzer. 96-well plates were coated with CellTak (Corning), washed, and air dried. T cells were plated in Seahorse XF DMEM Medium (Agilent) supplemented with 1% fetal bovine serum (FBS) and centrifuged for adherence. Next, 1μM oligomycin and 2μM rotenone/1μM antimycin A were injected sequentially, and the oxygen consumption rate (OCR) and extracellular acidification rate (ECAR) were measured. The mitochondrial ATP production rate was quantified based on the decrease in the OCR. The glycolytic ATP production rate was calculated as the increase in the ECAR combined with total proton efflux fate (PER). Seahorse XF Cell Mito Stress Test assays were performed as above and 1μM oligomycin, 1.5uM FCCP, and 2μM rotenone/1μM antimycin A were injected sequentially, and the oxygen consumption rate (OCR) was measured. Spare respiratory capacity was calculated as the difference between the basal and maximal OCR readings after addition of FCCP.

RNA analysis and UPR arrays

RNA as isolated with RNeasy Mini Kit (Qiagen, 74104) and concentration was measured using the SpectraDrop Micro-Volume Microplate (Molecular Devices). Single-strand cDNA was made with 500 ng RNA using the High-Capacity RNA-to-cDNA Kit (Applied Biosystems, 4387406, Thermo Fisher Scientific). TaqMan Gene Expression Array Plates (Thermo Fisher Scientific) were used to perform Unfolded Protein Response (UPR) arrays

using the StepOnePlus Real-Time PCR System (Applied Biosystems, Thermo Fisher Scientific). Gene expression was normalized using global normalization via the Thermo Fisher Connect Platform analysis software.

Metabolomics

Sample Preparation: Cells were harvested and washed with sodium chloride solution then resuspended in 80% methanol for multiple freeze-thaw cycles at −80°C and stored at −80°C overnight to precipitate the hydrophilic metabolites. Samples were centrifuged at 20,000xg and methanol was extracted for metabolite analysis. Remaining protein pellets were dissolved with 8M urea and total protein was quantified using BCA assay. Total protein amount was used for equivalent loading for High Performance Liquid Chromatography and High-Resolution Mass Spectrometry and Tandem Mass Spectrometry (HPLC-MS/MS) analysis.

Data Acquisition: Samples were dried with a SpeedVac then 50% acetonitrile was added for reconstitution followed by overtaxing for 30 sec. Sample solutions were centrifuged and supernatant was collected and analyzed by High-Performance Liquid Chromatography and High-Resolution Mass Spectrometry and Tandem Mass Spectrometry (HPLC-MS/MS). The system consists of a Thermo Q-Exactive in line with an electrospray source and an Ultimate3000 (Thermo) series HPLC consisting of a binary pump, degasser, and auto-sampler outfitted with a Xbridge Amide column (Waters; dimensions of 2.3 mm × 100 mm and a 3.5 µm particle size). The mobile phase A contained 95% (vol/vol) water, 5% (vol/vol) acetonitrile, 10 mM ammonium hydroxide, 10 mM ammonium acetate, pH = 9.0; B with 100% Acetonitrile. For gradient: 0 min, 15% A; 2.5 min, 30% A; 7 min, 43% A; 16 min, 62% A; 16.1-18 min, 75% A; 18-25 min, 15% A with flow rate of 150 µL/min. A capillary of the ESI source was set to 275 °C, with sheath gas at 35 arbitrary units, auxiliary gas at 5 arbitrary units and the spray voltage at 4.0 kV. In positive/negative polarity switching mode, an m/z scan range from 60 to 900 was chosen and MS1 data was collected at a resolution of 70,000. The automatic gain control (AGC) target was set at 1×10^6 and the maximum injection time were 200 ms. The top 5 precursor ions were subsequently fragmented, in a data-dependent manner, using the higher energy collisional dissociation (HCD) cell set to 30% normalized collision energy in MS2 at a resolution power of 17,500. Besides matching m/z, metabolites were identified by matching either retention time with analytical standards and/or MS2 fragmentation pattern. Metabolite acquisition and identification was carried out by Xcalibur 4.1 software (RRID: SCR_014593) and Tracefinder 4.1 software, respectively.

Statistical Analysis: Post identification, samples were normalized by taking the peak area under the curve for each metabolite per sample and dividing by the quotient of the total ion count (TIC) per sample over the lowest TIC in the batch. Subsequent transformation of normalized data was carried out with auto scaling to account for heteroscedasticity (23). Metabolites that were below detection in all samples were removed from analysis; missing values were imputed with 1/5 of the minimum positive value of their corresponding variable. Differential metabolite expression between groups of interest were identified through a combination of fold change >2 and raw p-value < 0.1 and visualized using a clustered heatmap. Overrepresentation enrichment analysis using the KEGG database

(RRID: SCR_012773) was performed on metabolites meeting this criterion to identify biological processes associated with differential expression (24). All statistical analysis was performed using the MetaboAnalyst 5.0 web server (RRID: SCR_015539) (25).

Statistical Analysis

GraphPad Prism v 9.3.0 (RRID: SCR_002798) was used to calculate p values with one-way analysis of variation (ANOVA) with a Dunnet's or Tukey's multiple comparison test where appropriate, unpaired two-sided Student's *t*-test or paired Student's *t*-test as indicated in the figure legend. For tumor growth curves, longitudinally measured tumor size was analyzed using linear mixed effects regression with factors for experimental condition, time (as a continuous variable), and their interaction, and mouse-specific random effects to account for the correlation among measures obtained from the same animal over time. Analysis was performed on the logarithmic scale to satisfy normality assumptions and to induce linearity over time. Group comparisons at specific time points were conducted using linear contrasts and limited to time points with ≥ 3 measurements per group. Analyses were performed using SAS 9.4 (RRID: SCR_008567) (Supplemental Table 1). Survival was calculated using Log-Rank, Mantel-Cox test of survival proportions. Values of $p < 0.05$ were considered significant. Numerical p values are indicated in the figures.

Data Availability Statement

The data generated in this study are available upon request from the corresponding author.

Results

Protein Synthesis is attenuated in tumor infiltrating T cells

Recent advances in single cell RNA (26) and ATAC sequencing (27) have allowed for identification of genetic and epigenetic traits associated with enhanced antitumor T cell function. However, the mechanisms responsible for controlling the translation of these instructions into effector functions have yet to be elucidated in antitumor immunity. We recently published an assay that allows monitoring protein synthesis on a per-cell basis (18). The fluorescent analogue of methionine, L-homopropargylglycine (L-HPG), is incorporated into new forming polypeptide chains and quantified by flow cytometry through Click-IT chemistry (1,28-30) (Fig 1A). Using this approach, we assessed global protein synthesis in endogenous CD8 T cells across multiple organs in B16 melanoma-bearing mice. Rates of translation were determined by normalizing to samples treated with translation inhibitor cycloheximide (CHX). Compared to splenic and tumor-draining lymph nodes (tDLN), tumor infiltrating CD8 T cells demonstrated a significant reduction in protein translation (Fig 1B). We replicated this phenomenon using freshly isolated human tumors from various cancer types and patient matched PBMCs suggesting that blunted protein synthesis is a common theme of tumor infiltrating CD8 T cells in both humans and mice (Fig 1C).

The TME consists of a heterogenous milieu of cell types and biochemical processes that coordinate to suppress T cells in both contact independent and dependent manners (31,32). To resolve the critical aspects restricting protein translation in the TME, we utilized a coculture assay in which tumor cells were seeded for 24 hours prior to introducing T cells

into transwell inserts for 36 hours (18) (Fig 1D). OT-1 T cells (Fig 1E) or normal human donor PBMC (Fig 1F) were activated and expanded with cognate OVA antigen or soluble CD3/28 activators, respectively. Thereafter, T cells were introduced into tumor or non-tumor seeded transwells for 36 hours (4) (18) and protein translation rates were measured. In both mouse and human T cells the presence of tumor significantly reduced protein translation rates (Fig 1E-F). The phenomenon was also apparent when human CD8 T cells were activated with soluble CD3/28 activators and expanded in supernatant from freshly isolated B16 tumors (Supplemental Figs. 1A-B). We further validated these observations using a second protein translation assay that incorporates O-propargyl-puromycin into the ribosomal A-site allowing for fluorescent labelling of nascent polypeptide chains (Supplemental Fig 2). We found that reduced translational capacity in T cells was a general phenomenon specific to tumor cell lines as coculture with both MC-38 Adenocarcinoma or MCA-205 Fibrosarcoma mimicked the B16 data. However, when cocultured with 293-T human embryonic kidney cells, T cells experienced minimal reduction in protein synthesis relative to control (Supplemental Fig 3). These data indicate that tumor cell-specific reduction in protein translation occurs in part through a contact independent mechanism.

Given that cytokine synthesis is a product of translation (33) we asked whether the reduction in translation in the TME corresponded with diminished cytotoxic cytokine synthesis. Upon coculture with tumor cells, CD3/28 activated human PBMCs displayed reduced TNFα/IFNγ production (Fig 1G). Pretreating cells with CHX prior to restimulation resulted in abrogation of TNFα/IFNγ in control and TME CD8 PBMCs, indicating the requirement of continuous translation for cytokine synthesis. Cytokine production in the presence of tumor cells was also reduced using the OT-1 system, further validating our findings (Supplemental Fig 4). Our data illustrate that soluble factors or competition with tumor cells induce decreased translation, and more specifically cytokine synthesis in CD8 T cells.

Glucose stress undermines T cell translation

Protein translation at the magnitude seen in effector T cell activation and expansion is a metabolically intensive process requiring ATP (21,34). A common stressor impacting T cell function in solid tumors is competition for exogenous glucose (5). Given that glucose fuels effector cell metabolism, in addition to the contact independent nature of our above findings, we asked whether glucose competition could drive the reduction in protein synthesis in T cells. Incremental increases in tumor cell numbers resulted in a stepwise reduction in environmental glucose in coculture media (Fig 2A). This was coupled with an identical graded reduction in protein synthesis, IFNγ, and TNFα production (Fig 2B-D) highlighting the link between glucose availability and CD8 T cell functional capacity. Exposure to low glucose associated with TME pressure in the coculture system resulted in a significant reduction in ATP output from glycolysis (glycoATP) and mitochondria-linked ATP (mitoATP) in OT-1 mouse and purified human CD8 T cells as measured by Seahorse Bioanalysis ATP rate assay (Fig 2E-F). The data indicate that competition for glucose significantly alters T cell metabolism, thereby limiting T cell effector function.

We next performed a series of rescue or removal experiments to confirm the necessity of glucose in sustaining protein translation in TME stress. By supplementing the T cell-tumor

cell coculture media with exogenous glucose we restored glycolytic ATP to no tumor controls levels (Fig 2G). In line with this, exogenous glucose rescued protein translation rates in the presence of tumor cells (Fig 2H). We next inhibited glycolysis in T cells in the transwell coculture system by adding 2-deoxy-glucose (2DG) 2 hours prior to measurement of protein translation. 2DG is taken up by cell glucose transporters (35) and competitively inhibits generation of glucose-6-phosphate in the second step of glycolysis. Seahorse bioanalysis indicated a reduction in glycoATP (Fig 2I) in all 2DG conditions irrespective of tumor cells, validating acute treatment with 2DG blunts glycolysis. We also noted a significant reduction in translation rate in T cells treated with 2DG compared to vehicle control irrespective of tumor presence (Fig 2J). Combined, these data highlight the importance of exogenous glucose in dictating T cell metabolic programming, protein translation, and effector function.

p-eIF2α attenuates T cell translation and tumor control

Metabolic perturbations such as low glucose environments lead to disturbances in protein folding in the ER (36). In response, the ER stress sensor PKR ER-like kinase (PERK) can mediate phosphorylation of eIF2α at Ser51 (37,38) which reduces global translation in favor of maintaining proteostasis (39). We found that OT-1 CD8 T cells exposed to low glucose conditions *in vitro* demonstrated a significant increase in p-eIF2α at Ser51 compared to normal glucose controls (Supplemental Fig 5). Upon coculture with ascending numbers of tumor cells we noted a stepwise induction of eIF2α phosphorylation that was significantly correlated with the graded reduction in protein translation (Fig 3A) that resulted in the depression of cytokine synthesis previously observed (Fig 2). Along with eIF2α phosphorylation, we observed enrichment of PERK axis proteins ATF4, CHOP, and ERO1α (Fig 3B), indicating PERK could be upstream of p-eIF2α in T cells. Gene expression data generated from a targeted UPR gene array also suggested upregulation of PERK-directed genes *Ddit3* (CHOP) and *Ero1l* (Fig 3C) in T cells exposed to tumor cell pressure.

To determine the contribution of PERK to eIF2α phosphorylation and translation attenuation in TME stress, we generated a TCR transgenic T cell specific PERK knockout mouse by crossing OT-1 mice bearing a *cre* under the LCK promoter and loxp sites flanking exons 7-9 of the PERK gene. T cells from resulting wild type (OT-1 LCK-*cre(−)* PERK$^{f/f}$; WT) or PERK KO mice (OT-1 LCK-cre(+) PERK$^{f/f}$; PKO) were activated with cognate antigen then introduced into the coculture transwell system. p-eIF2α was absent in PKO cells harvested from control and tumor-seeded transwells (Fig 3D), indicating that PERK is the dominant ER stress sensor to mediate eIF2α phosphorylation in T cells responding to tumor pressure. In line with this, translation attenuation was diminished in PKO T cells exposed to tumor stress (Fig 3E). Interestingly, at baseline PKO T cells displayed reduced protein synthesis relative to WT cells, indicating that other facets of PERK biology could regulate T cell translation in non-stressed controls.

Next, we asked whether p-eIF2α was the direct arbiter of translation attenuation in T cells exposed to the TME. We backcrossed TCR transgenic OT-1 mice to mice bearing a single amino acid substitution of serine to alanine at codon 51 (S51A) in the phosphorylation site of the eIF2α protein (3). Animals homozygous for S51A mutation die near birth due

to defective gluconeogenesis, thus we studied p-eIF2α regulation in mice bearing T cells heterozygous for the S51A mutation (eIF2α$^{S51A+/-}$). Western blotting indicated a reduction in p-eIF2α in eIF2α$^{S51A+/-}$ T cells exposed to TME stress (Fig 3F) that correlated with an increase in translational capacity relative to littermate controls (Fig 3G). Phenotypic analysis by spectral flow cytometry uncovered subtle changes between WT and eIF2α$^{S51A+/-}$ T cells harvested from control and tumor-seeded transwells. eIF2α$^{S51A+/-}$ T cells showed a reduction in CD62L in control and tumor-seeded transwells that was accompanied by TME-specific increases in PD-1 and CTLA-4 as well as a surprising increase in TCF-1 expression, suggesting that p-eIF2α-mediated translation is linked to T cell activation and stemness in stress (Supplemental Fig 6).

Given that we have previously reported the ability to sustain translation in tumors propels T cell tumor control (18), we aimed to test the effect of sustained translation, mediated by loss of PERK or p-eIF2α, on antitumor immunity. Subcutaneous B16-OVA melanomas were established in C57BL/6 mice and WT, PKO, or eIF2α$^{S51A+/-}$ OT-1 T cells were infused to mice bearing 7-day established tumors. We observed that PKO and eIF2α$^{S51A+/-}$ T cells induced superior tumor control compared to WT-matched controls (Fig 3H-I). Our findings illustrate that the PERK-p-eIF2α axis reduces translational capacity and tumor control of T cells.

Metabolic reprogramming alleviates translation attenuation

A paradigm exists whereby T cells metabolically reprogrammed away from exogenous glucose dependency display heightened tumor control marked by amplified cytotoxic cytokine production (15,16). We next asked whether relief of glucose stress through metabolic remodeling mitigates translation attenuation as a means to sustain antitumor T cell function. We administered acute (2 hour) or chronic (36 hour) 2DG to OT-1 T cells seeded in the tumor transwell coculture. We first assessed the effect of 2DG treatment on T cells through in-depth phenotypic analysis. While chronic 2DG reduced T cell expansion *in vitro* (Supplemental Fig 7A) this was not a result of apoptosis as Annexin V staining and cell viability were not significantly different across groups (Supplemental Figs. 7B-C). High dimensional spectral flow cytometry analysis revealed that chronic 2DG treatment resulted in a significant increase in memory like T cell markers such as CD44, CD62L, TCF1, and CD69 coupled with a reduction in effector specific markers including Granzyme B and Ki67 (Supplemental Fig 7D-I). Furthermore, while IFNγ staining intensity was similar across groups, there was a significant increase in TNFα synthesis suggesting chronic 2DG treatment enhanced the polyfunctionality of T cells (Supplemental Fig 7J-K). These findings align with previous data showing chronic 2DG treatment skews T cells towards a memory like phenotype (16). We next investigated the extent to which the metabolic reprogramming strategy altered stress mediated translation attenuation. Western blotting revealed a pronounced reduction in p-eIF2α in chronic compared to acute 2DG treatment or vehicle control (Fig 4A). Moreover, chronic 2DG remodeling prompted elevated translation in T cells experiencing TME nutrient deprivation (Fig 4B-C) relative to non-tumor controls. Seahorse bioanalysis indicated an increase in glycolytic and mitochondrial ATP output in chronic 2DG treated T cells under tumor stress (Fig 4D-E), suggesting complete metabolic reprogramming that supported energy production in nutrient stress.

The possibility exists that T cell translation was bolstered by an adverse effect of chronic 2DG on tumor cells. As chronic 2DG conditioning promotes stem-like memory T cell development (Supplemental Fig 7), we next sought to validate elevated translation in TME stress was a property of metabolic remodeling of T cells to the memory lineage by using the cytokine IL-15 to generate memory cells (Supplemental Fig 8). Similar to chronic 2DG treatment, IL-15 memory-like T cells harvested from the tumor transwell coculture assay displayed a significant reduction in p-eIF2α compared to IL-2 effectors (Fig 4F). Furthermore, when comparing IL-15 and IL-2 treated T cells exposed to the TME we saw a substantial downregulation of global UPR genes in IL-15-conditioned T cells (Fig 4G), including those within the PERK axis (*Eif2a, Atf4, Ero1l*). Similar to chronic 2DG-treated T cells, IL-15 skewing enhanced protein translation rates in both non-tumor and tumor conditions (Fig 4H-I) and produced a marked increase in ATP production in the presence of tumor pressure (Fig 4J-K). These data demonstrate that metabolic reprogramming coupled to memory-like T cell differentiation alleviates p-eif2α translation attenuation.

Proteasome function sustains translation and tumor immunity

We next aimed to elucidate the intracellular mechanism that safeguards memory-like T cells from translation attenuation. Several studies have suggested that accelerated protein degradation is a component of memory cell metabolism (22,40). Given that optimal protein synthesis requires a delicate balance between protein degradation and translation (41), we asked whether the proteasome could be responsible for mitigating translation attenuation in memory-like T cells exposed to TME stress. We utilized a probe with fluorescent activity proportional to proteasome subunit activation (22,42) to assess proteasome activity in T cells. In tumor-seeded cocultures, IL-15-primed T cells displayed an increase in the frequency of proteasome activity^{high} cells relative to IL-2 effectors that was extinguished in the presence of proteasome inhibitor MG132 (Fig 5A). Western blotting of IL-15-primed T cells revealed a substantial induction of p-eIF2α upon MG132 treatment (Fig 5B) that correlated with a robust reduction in translation (Fig 5C). These data suggest that proteasome function is required to overcome translation attenuation in T cells exposed to nutrient stress.

We next sought to address the mechanism by which the proteasome sustains optimal T cell function. Given that proteasome-mediated protein degradation supports ATP synthesis in cells experiencing nutrient stress (43), we asked whether the proteasome was involved in metabolic remodeling of IL-15 primed cells. Proteasome inhibition induced a reduction in glycolytic and mitochondrial ATP in IL-15 conditioned T cells in tumor-seeded transwells (Fig 5D-E). Metabolomic profiling of IL-15-conditioned cells in tumor stress treated with vehicle or MG132 identified 32 significantly enriched metabolites in IL-15 T cells related to proteasome activity (Fig 5F). Pathway enrichment analysis of these metabolites showed upregulation of processes fundamental for memory T cell mediated tumor control such as gluconeogenesis and glutathione metabolism (44). The data also evidenced a significant enrichment in aminoacyl-tRNA biosynthesis, further supporting a role for the proteasome as an integral component of sustained protein translation in the TME (Fig 5G, Supplemental Fig 9). Taken together, these data indicate that the proteasome plays a critical role in supporting a metabolic profile necessary for increased T cell tumor immunity.

Functionally, IL-15 conditioned T cells are of interest to the immunotherapy field due to their robust and prolonged levels of tumor control relative to effectors. IL-15 conditioning has been shown to enhance CAR T cell therapy (45) and improve response to checkpoint blockade (46). Thus, we tested whether access to proteasome mediated protein degradation was a molecular checkpoint required for tumor control in memory-like T cells. Mice bearing B16F1-OVA melanomas were infused with IL-15-conditioned T cells treated with vehicle or MG132 for four hours prior to infusion and tumor growth was assessed. While IL-15-conditioned T cells generated potent tumor control, IL-15-conditioned T cells unable to access the proteasome showed reduced tumor control and diminished survival benefits (Fig 5H-I).

Proteasome stimulation enhances T cell tumor immunity

While MG132 is a potent and selective inhibitor of proteasome function, we sought to conclusively demonstrate the importance of proteasome function through use of pharmacologic stimulators. Cyclosporine A (CsA), most commonly used as an immunosuppressant, has proteasome stimulating properties which drive memory cell development (22). Using the fluorescent activity probe, we validated that CsA treatment increased proteasome function of naïve CD8 splenocytes (Fig 6A). We next tested whether proteasome stimulation increased protein translation. CsA conditioning produced a marked reduction in p-eIF2α expression (Fig 6B) and a significant increase in protein synthesis in T cells harvested from the tumor transwell coculture assay (Fig 6C). The observation that proteasome activity was heightened in memory-like T cells (Fig 5) prompted us to assess the phenotype of CsA-conditioned OT1 T cells. We observed that CsA generated T cells with memory traits such as high CD62L and Bcl2 expression coupled with reduced proliferative capacity marked by Ki-67. (Supplemental Fig 10A-C). These findings were replicated using a low affinity physiologically relevant CD8 TCR-transgenic model, the pmel-gp100 system, indicating that proteasome stimulation could be used to shape T cell fate across a range of TCR-peptide affinities (Supplemental Fig 10D-F). Combined with our above findings, these data demonstrate that proteasome activity is necessary and sufficient to protect from translation attenuation in T cells responding to TME stress.

We sought to address the viability of proteasome stimulation as an interventional strategy to improve the efficacy of adoptively transferred T cells to control solid tumors in mice. OT-1 T cells were activated with OVA peptide then conditioned in the presence of CsA or vehicle prior to infusion into B16-OVA-bearing mice. CsA treatment enhanced T cell tumor control resulting in extended animal survival (Fig 6D-E). Next, we performed a similar ACT experiment in which tumors were harvested five days post T cell infusion and donor T cells in tumors were assessed. CsA treatment significantly enhanced the percentage of live donor OT1 T cells that accrued in B16-F1-OVA melanomas relative to controls (Fig 6F). CsA treatment also augmented the frequency of IFNγ-TNFα polyfunctional OT-1 T cells in tumors (Supplemental Fig 11). Using pmel T cells infused into mice bearing B16-F1 melanomas, we validated that CsA treatment induced a robust increase in percentage of live donor CD8 T cells accruing in tumors responding with lower affinity to a physiologically relevant melanoma antigen (Fig 6G). Collectively, the data suggest that proteasome activity promotes CD8 TIL survival in tumors, augmenting immunity in TME stress.

Discussion

Apart from primary translation of mRNA to amino acid chains, protein synthesis also requires successful folding of secondary, tertiary, and quaternary structures (47). Early studies estimated that 70% of the ATP reservoirs are required to sustain translation, making it one of the most bioenergetically taxing cellular processes (48). For T cells, antigenic stimulation activates a dynamic process highlighted by a translation rate of approximately 800,000 proteins per minute (40). Thus, it is not challenging to recognize the substantial metabolic burden on T cells, particularly in a scenario such as the TME where competition for nutrients and global cell stressors are exceptional (5). Despite this, very little is known about the underlying mechanisms required to support translation in the TME. We show here that blunted protein synthesis is a hallmark of tumor infiltrating CD8 T cells driven by phosphorylation of eIF2α . These findings are a departure from previous studies of ER stress in two ways. First, we demonstrate that the TME represents a biologically relevant model to investigate ER stress in lieu of chemical insult. Second, to our knowledge, this is the first study to establish the antitumor capacity of T cells is directly related to their ability resolve intrinsic protein stress. Thus, these findings implicate T cell translation attenuation as a previously unappreciated molecular checkpoint that dictates effective immunotherapy.

The metabolic demands of T cells are directly related to their differentiation state and predictive of their effector function (49). Naïve T cells rely on oxidative phosphorylation, activated effector cells are highly glycolytic, and memory T cells employ *de novo* fatty acid (FA) synthesis and FA β oxidation (50), whereas exhausted tumor infiltrating CD8s display poor mitochondrial health associated with depressed bioenergetic output (49). The dependence on exogenous glucose represents a significant vulnerability to tumor infiltrating T cells, and work has conclusively demonstrated that metabolic reprogramming enhances cytokine production and, by extension, antitumor immunity (15,16). Our results here elaborate on those studies, suggesting that extinguished cytokine synthesis in the TME is a side effect of global translation repression. Given the widespread interest in metabolic reprogramming as an interventional approach, the extent to which these strategies relieve ER stress should be further elucidated. Indeed, the concepts uncovered can be extended to recent work highlighting systemic Interleukin-10-Fc fusion protein therapy cytokine therapy rehabilitates the terminally exhausted CD8 tumor infiltrating population through reestablishing metabolic health, as connections between ER stress, the UPR, and exhausted T cells have not been made (51).

Stress mediated global translation attenuation serves to restore proteostasis by enabling degradation of misfolded proteins via the ubiquitin-proteasome pathway (41,52). As stress persists the cell compensates by increasing expression of oxidative protein folding machinery, resulting in the unintended consequence of cell reactive oxygen species generation (53,54). Work from our group and others has illustrated that such oxidative stress is a trait of terminally exhausted T cells, (10,55) however, the concept of a misfolded protein burden in relation to T cell exhaustion is relatively unexplored concept. Here we found that metabolic reprogramming overcomes TME-mediated translation attenuation in a manner that is dependent on proteasome mediated protein degradation. Metabolic reprogramming strategies have been shown to alleviate oxidative stress in T cells in tumors

through invigoration of antioxidant systems (44). Our data indicate for the first time that the potential to protect T cells from accrual of misfolded proteins is intimately tied to engagement of antioxidant metabolism and linked by the proteasome. While proteasome activation directly mitigates translation attenuation (56), our metabolomic data suggest that proteasome activity also fuels pathways associated with intracellular detoxification such as gluconeogeneic and glutathione metabolism (57), necessary for superior T cell tumor control (44). While the direct contribution of the 26S or immunoproteasome to program T cell antitumor metabolism requires further elucidation, our data strongly suggest proteasome stimulation as a new method for enhancing immunotherapy outcomes.

While this study illustrates a significant defect in protein translation in T cells during the initial phase of B16 melanoma growth and in multiple human tumor types, there were significant limitations in the study approach that can be rectified in future works. Firstly, the *in vitro* transwell coculture assay did not replicate persistent antigen stimulation that leads to T cell exhaustion. The copper-based fixation required to monitor protein translation with HPG at the single cell level, while innovative, makes it difficult to deeply phenotype protein synthesis in T cell subsets based on limited availability of resistant fluorochromes. Future work should aim to simultaneously profile translation rates in T cell subsets, the myeloid compartment, and tumor cells *in vivo*. These data could elucidate translation as the end-game of the metabolic tug-of-war in the tumor microenvironment for glucose, amino acids, and fats for bioenergetic fuel. A second substantial limitation of our *in vitro* approach was that it is difficult to test whether glucose (or amino acid) competition as a mechanism that impairs T cell translation was unique to the T cell-tumor interaction. It is likely that any two proliferative, metabolically active cell types will compete for exogenous nutrients. However, as was a focus of this work, a clear picture has emerged that the battle between T and tumor cells for resources is particularly pertinent in the environment of tumors as it critically defines tumor growth or regression.

Supplementary Material

Refer to Web version on PubMed Central for supplementary material.

Acknowledgements

Metabolomics services were performed by the Metabolomics Core Facility at Robert H. Lurie Comprehensive Cancer Center of Northwestern University. Biostatistics work is supported in part by the Biostatistics Shared Resource, Hollings Cancer Center, Medical University of South Carolina (P30 CA138313). Financial support from NCI/NIH is as follows: R01CA244361-01A1, R01CA248359-01 (JET), T32 5T32AI132164-04 (BPR), T32 DE01755 (MDT), T32 CA 193201 (AMA). We are grateful to Drs. Denis Guttridge and Albert Baldwin at the Medical University of South Carolina and University of North Carolina at Chapel Hill, respectively, for providing thoughtful guidance on manuscript development and submission.

Financial Support:

R01CA244361-01A1, R01CA248359-01 (JET), T32 5T32AI132164-04 (BPR), T32 DE01755 (MDT), T32 CA 193201 (AMA), P30 CA138313 (EGH)

References

1. Araki K, Morita M, Bederman AG, Konieczny BT, Kissick HT, Sonenberg N, et al. Translation is actively regulated during the differentiation of CD8(+) effector T cells. Nat Immunol 2017;18:1046–57 [PubMed: 28714979]
2. Holcik M Could the eIF2α-Independent Translation Be the Achilles Heel of Cancer? Frontiers in Oncology 2015;5
3. Scheuner D, Song B, McEwen E, Liu C, Laybutt R, Gillespie P, et al. Translational control is required for the unfolded protein response and in vivo glucose homeostasis. Mol Cell 2001;7:1165–76 [PubMed: 11430820]
4. Bian Y, Li W, Kremer DM, Sajjakulnukit P, Li S, Crespo J, et al. Cancer SLC43A2 alters T cell methionine metabolism and histone methylation. Nature 2020;585:277–82 [PubMed: 32879489]
5. Chang CH, Qiu J, O'Sullivan D, Buck MD, Noguchi T, Curtis JD, et al. Metabolic Competition in the Tumor Microenvironment Is a Driver of Cancer Progression. Cell 2015;162:1229–41 [PubMed: 26321679]
6. Thevenot PT, Sierra RA, Raber PL, Al-Khami AA, Trillo-Tinoco J, Zarreii P, et al. The stress-response sensor chop regulates the function and accumulation of myeloid-derived suppressor cells in tumors. Immunity 2014;41:389–401 [PubMed: 25238096]
7. Brand A, Singer K, Koehl GE, Kolitzus M, Schoenhammer G, Thiel A, et al. LDHA-Associated Lactic Acid Production Blunts Tumor Immunosurveillance by T and NK Cells. Cell Metab 2016;24:657–71 [PubMed: 27641098]
8. Andrews AM, Tennant MD, Thaxton JE. Stress relief for cancer immunotherapy: implications for the ER stress response in tumor immunity. Cancer Immunol Immunother 2020
9. Harding HP, Zhang Y, Bertolotti A, Zeng H, Ron D. Perk is essential for translational regulation and cell survival during the unfolded protein response. Mol Cell 2000;5:897–904 [PubMed: 10882126]
10. Hurst KE, Lawrence KA, Essman MT, Walton ZJ, Leddy LR, Thaxton JE. Endoplasmic Reticulum Stress Contributes to Mitochondrial Exhaustion of CD8(+) T Cells. Cancer Immunol Res 2019;7:476–86 [PubMed: 30659052]
11. Cao Y, Trillo-Tinoco J, Sierra RA, Anadon C, Dai W, Mohamed E, et al. ER stress-induced mediator C/EBP homologous protein thwarts effector T cell activity in tumors through T-bet repression. Nat Commun 2019;10:1280 [PubMed: 30894532]
12. Cham CM, Gajewski TF. Glucose availability regulates IFN-gamma production and p70S6 kinase activation in CD8+ effector T cells. J Immunol 2005;174:4670–7 [PubMed: 15814691]
13. Grasmann G, Smolle E, Olschewski H, Leithner K. Gluconeogenesis in cancer cells – Repurposing of a starvation-induced metabolic pathway? Biochimica et Biophysica Acta (BBA) - Reviews on Cancer 2019;1872:24–36 [PubMed: 31152822]
14. Cabodevilla AG, Sánchez-Caballero L, Nintou E, Boiadjieva VG, Picatoste F, Gubern A, et al. Cell survival during complete nutrient deprivation depends on lipid droplet-fueled β-oxidation of fatty acids. J Biol Chem 2013;288:27777–88 [PubMed: 23940052]
15. Klein Geltink RI, Edwards-Hicks J, Apostolova P, O'Sullivan D, Sanin DE, Patterson AE, et al. Metabolic conditioning of CD8(+) effector T cells for adoptive cell therapy. Nat Metab 2020;2:703–16 [PubMed: 32747793]
16. Sukumar M, Liu J, Ji Y, Subramanian M, Crompton JG, Yu Z, et al. Inhibiting glycolytic metabolism enhances CD8+ T cell memory and antitumor function. J Clin Invest 2013;123:4479–88 [PubMed: 24091329]
17. van der Windt GJ, O'Sullivan D, Everts B, Huang SC, Buck MD, Curtis JD, et al. CD8 memory T cells have a bioenergetic advantage that underlies their rapid recall ability. Proc Natl Acad Sci U S A 2013;110:14336–41 [PubMed: 23940348]
18. Hurst KE, Lawrence KA, Robino RA, Ball LE, Chung D, Thaxton JE. Remodeling Translation Primes CD8(+) T-cell Antitumor Immunity. Cancer Immunol Res 2020;8:587–95 [PubMed: 32075802]
19. Rousseau A, Bertolotti A. Regulation of proteasome assembly and activity in health and disease. Nature Reviews Molecular Cell Biology 2018;19:697–712 [PubMed: 30065390]

20. Obeng EA, Carlson LM, Gutman DM, Harrington WJ, Jr., Lee KP, Boise LH. Proteasome inhibitors induce a terminal unfolded protein response in multiple myeloma cells. Blood 2006;107:4907–16 [PubMed: 16507771]
21. Wolf T, Jin W, Zoppi G, Vogel IA, Akhmedov M, Bleck CKE, et al. Dynamics in protein translation sustaining T cell preparedness. Nature Immunology 2020;21:927–37 [PubMed: 32632289]
22. Widjaja CE, Olvera JG, Metz PJ, Phan AT, Savas JN, de Bruin G, et al. Proteasome activity regulates CD8+ T lymphocyte metabolism and fate specification. J Clin Invest 2017;127:3609–23 [PubMed: 28846070]
23. van den Berg RA, Hoefsloot HCJ, Westerhuis JA, Smilde AK, van der Werf MJ. Centering, scaling, and transformations: improving the biological information content of metabolomics data. BMC Genomics 2006;7:142 [PubMed: 16762068]
24. Xia J, Wishart DS. MSEA: a web-based tool to identify biologically meaningful patterns in quantitative metabolomic data. Nucleic Acids Research 2010;38:W71–W7 [PubMed: 20457745]
25. Pang Z, Chong J, Zhou G, de Lima Morais DA, Chang L, Barrette M, et al. MetaboAnalyst 5.0: narrowing the gap between raw spectra and functional insights. Nucleic Acids Research 2021
26. Miller BC, Sen DR, Al Abosy R, Bi K, Virkud YV, LaFleur MW, et al. Subsets of exhausted CD8(+) T cells differentially mediate tumor control and respond to checkpoint blockade. Nat Immunol 2019;20:326–36 [PubMed: 30778252]
27. Shin HM, Kim G, Kim S, Sim JH, Choi J, Kim M, et al. Chromatin accessibility of circulating CD8+ T cells predicts treatment response to PD-1 blockade in patients with gastric cancer. Nature Communications 2021;12:975
28. Graczyk D, White RJ, Ryan KM. Involvement of RNA Polymerase III in Immune Responses. Mol Cell Biol 2015;35:1848–59 [PubMed: 25776554]
29. Lai CP, Kim EY, Badr CE, Weissleder R, Mempel TR, Tannous BA, et al. Visualization and tracking of tumour extracellular vesicle delivery and RNA translation using multiplexed reporters. Nat Commun 2015;6:7029 [PubMed: 25967391]
30. Best MD. Click chemistry and bioorthogonal reactions: unprecedented selectivity in the labeling of biological molecules. Biochemistry 2009;48:6571–84 [PubMed: 19485420]
31. Anderson KG, Stromnes IM, Greenberg PD. Obstacles Posed by the Tumor Microenvironment to T cell Activity: A Case for Synergistic Therapies. Cancer Cell 2017;31:311–25 [PubMed: 28292435]
32. Whiteside TL. The tumor microenvironment and its role in promoting tumor growth. Oncogene 2008;27:5904–12 [PubMed: 18836471]
33. Scheu S, Stetson DB, Reinhardt RL, Leber JH, Mohrs M, Locksley RM. Activation of the integrated stress response during T helper cell differentiation. Nat Immunol 2006;7:644–51 [PubMed: 16680145]
34. Hershey JW, Sonenberg N, Mathews MB. Principles of translational control: an overview. Cold Spring Harb Perspect Biol 2012;4
35. Aft RL, Zhang FW, Gius D. Evaluation of 2-deoxy-D-glucose as a chemotherapeutic agent: mechanism of cell death. British Journal of Cancer 2002;87:805–12 [PubMed: 12232767]
36. Hsu SK, Chiu CC, Dahms HU, Chou CK, Cheng CM, Chang WT, et al. Unfolded Protein Response (UPR) in Survival, Dormancy, Immunosuppression, Metastasis, and Treatments of Cancer Cells. Int J Mol Sci 2019;20
37. Sudhakar A, Ramachandran A, Ghosh S, Hasnain SE, Kaufman RJ, Ramaiah KV. Phosphorylation of serine 51 in initiation factor 2 alpha (eIF2 alpha) promotes complex formation between eIF2 alpha(P) and eIF2B and causes inhibition in the guanine nucleotide exchange activity of eIF2B. Biochemistry 2000;39:12929–38 [PubMed: 11041858]
38. Muaddi H, Majumder M, Peidis P, Papadakis AI, Holcik M, Scheuner D, et al. Phosphorylation of eIF2alpha at serine 51 is an important determinant of cell survival and adaptation to glucose deficiency. Mol Biol Cell 2010;21:3220–31 [PubMed: 20660158]
39. Ron D, Walter P. Signal integration in the endoplasmic reticulum unfolded protein response. Nat Rev Mol Cell Biol 2007;8:519–29 [PubMed: 17565364]
40. Wolf T, Jin W, Zoppi G, Vogel IA, Akhmedov M, Bleck CKE, et al. Dynamics in protein translation sustaining T cell preparedness. Nat Immunol 2020;21:927–37 [PubMed: 32632289]

41. Labbadia J, Morimoto RI. The biology of proteostasis in aging and disease. Annu Rev Biochem 2015;84:435–64 [PubMed: 25784053]
42. Berkers CR, van Leeuwen FW, Groothuis TA, Peperzak V, van Tilburg EW, Borst J, et al. Profiling proteasome activity in tissue with fluorescent probes. Mol Pharm 2007;4:739–48 [PubMed: 17708652]
43. Huang H, Zhang X, Li S, Liu N, Lian W, McDowell E, et al. Physiological levels of ATP negatively regulate proteasome function. Cell Res 2010;20:1372–85 [PubMed: 20805844]
44. Ma R, Ji T, Zhang H, Dong W, Chen X, Xu P, et al. A Pck1-directed glycogen metabolic program regulates formation and maintenance of memory CD8(+) T cells. Nat Cell Biol 2018;20:21–7 [PubMed: 29230018]
45. Chen Y, Sun C, Landoni E, Metelitsa L, Dotti G, Savoldo B. Eradication of Neuroblastoma by T Cells Redirected with an Optimized GD2-Specific Chimeric Antigen Receptor and Interleukin-15. Clin Cancer Res 2019;25:2915–24 [PubMed: 30617136]
46. Wrangle JM, Velcheti V, Patel MR, Garrett-Mayer E, Hill EG, Ravenel JG, et al. ALT-803, an IL-15 superagonist, in combination with nivolumab in patients with metastatic non-small cell lung cancer: a non-randomised, open-label, phase 1b trial. Lancet Oncol 2018;19:694–704 [PubMed: 29628312]
47. Waudby CA, Dobson CM, Christodoulou J. Nature and Regulation of Protein Folding on the Ribosome. Trends Biochem Sci 2019;44:914–26 [PubMed: 31301980]
48. Pontes MH, Sevostyanova A, Groisman EA. When Too Much ATP Is Bad for Protein Synthesis. J Mol Biol 2015;427:2586–94 [PubMed: 26150063]
49. Zhang L, Romero P. Metabolic Control of CD8(+) T Cell Fate Decisions and Antitumor Immunity. Trends Mol Med 2018;24:30–48 [PubMed: 29246759]
50. O'Sullivan D, van der Windt GJ, Huang SC, Curtis JD, Chang CH, Buck MD, et al. Memory CD8(+) T cells use cell-intrinsic lipolysis to support the metabolic programming necessary for development. Immunity 2014;41:75–88 [PubMed: 25001241]
51. Guo Y, Xie YQ, Gao M, Zhao Y, Franco F, Wenes M, et al. Metabolic reprogramming of terminally exhausted CD8(+) T cells by IL-10 enhances anti-tumor immunity. Nat Immunol 2021;22:746–56 [PubMed: 34031618]
52. Hipp MS, Kasturi P, Hartl FU. The proteostasis network and its decline in ageing. Nat Rev Mol Cell Biol 2019;20:421–35 [PubMed: 30733602]
53. Han J, Back SH, Hur J, Lin YH, Gildersleeve R, Shan J, et al. ER-stress-induced transcriptional regulation increases protein synthesis leading to cell death. Nat Cell Biol 2013;15:481–90 [PubMed: 23624402]
54. Marciniak SJ, Yun CY, Oyadomari S, Novoa I, Zhang Y, Jungreis R, et al. CHOP induces death by promoting protein synthesis and oxidation in the stressed endoplasmic reticulum. Genes Dev 2004;18:3066–77 [PubMed: 15601821]
55. Vardhana SA, Hwee MA, Berisa M, Wells DK, Yost KE, King B, et al. Impaired mitochondrial oxidative phosphorylation limits the self-renewal of T cells exposed to persistent antigen. Nat Immunol 2020;21:1022–33 [PubMed: 32661364]
56. Meusser B, Hirsch C, Jarosch E, Sommer T. ERAD: the long road to destruction. Nat Cell Biol 2005;7:766–72 [PubMed: 16056268]
57. Mak TW, Grusdat M, Duncan GS, Dostert C, Nonnenmacher Y, Cox M, et al. Glutathione Primes T Cell Metabolism for Inflammation. Immunity 2017;46:1089–90 [PubMed: 28636957]

Significance Statement

Proteasome function is a necessary cellular component for endowing T cells with tumor killing capacity by mitigating translation attenuation resulting from the unfolded protein response induced by stress in the tumor microenvironment.

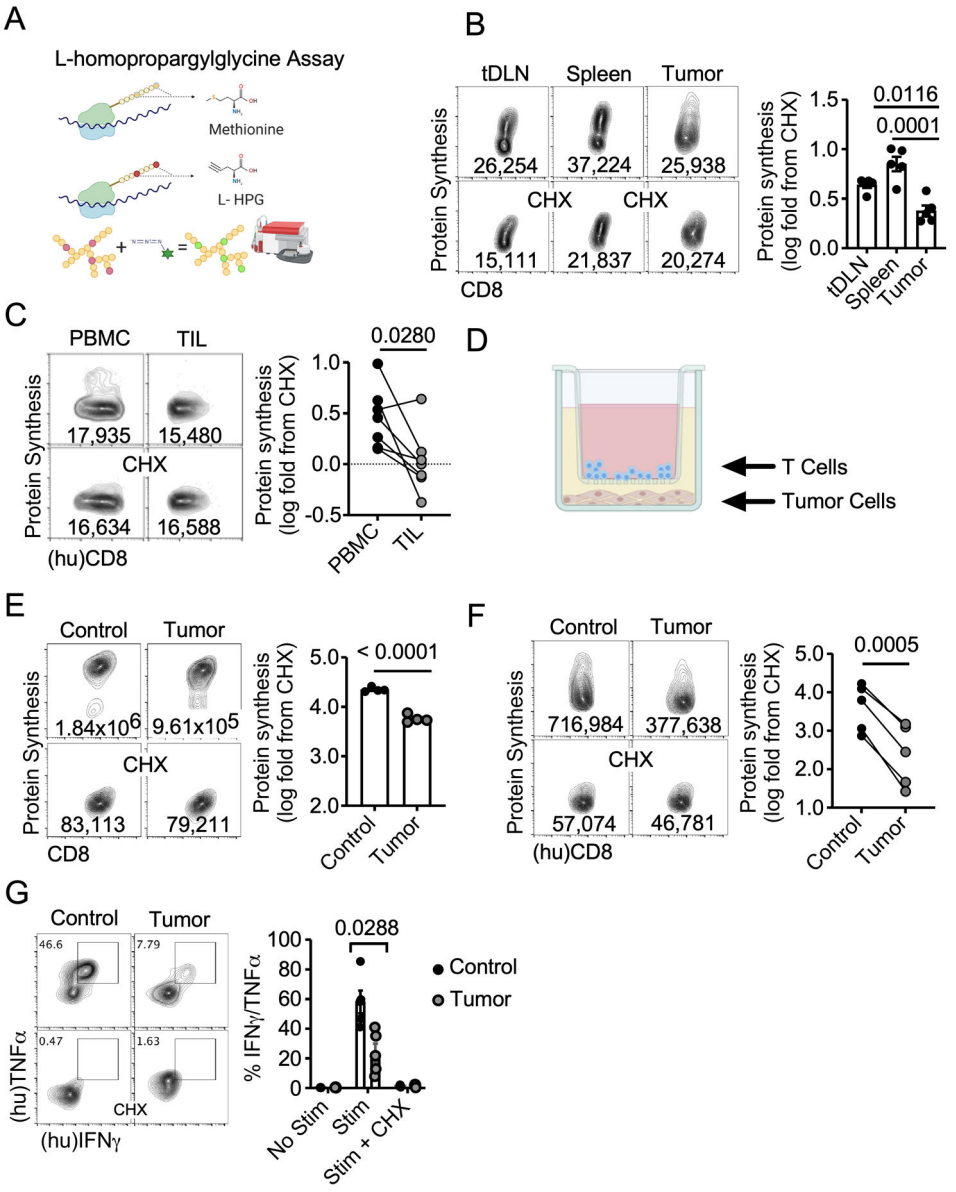

Figure 1. Protein synthesis is attenuated in tumor infiltrating T cells

A) Schematic representation of flow cytometry-based L-homopropargylglycine Assay to measure protein translation. Representative FACS plots and quantification of protein synthesis rates in **B**) endogenous CD8+ tDLNs, splenocytes, and TILs from B16F1 tumor-bearing mice (n=5 mice) and **C**) CD8+ TILs and autologous PBMC from n=7 untreated pleiomorphic undifferentiated sarcoma (3), metastatic (bone) renal cell, multiple myeloma (1), breast (1), and melanoma (1) patients. **D**) Graphic of tumor-T cell contact independent transwell coculture assay. Representative FACS plots and quantification of protein synthesis rates from **E**) OT-1 splenocytes stimulated with OVA peptide or **F**) CD8+ PBMC activated with CD3/28 activators as (n=5 donors) in the tumor-T cell transwell coculture. **G**) Representative FACS plots and quantification of IFNγ and TNFα production from CD8+ PBMC activated with CD3/28 activators (n=5 donors) in the tumor-T cell transwell assay

followed by PMA/Ionomycin stimulation ± pretreatment with protein synthesis inhibitor cycloheximide (CHX). Data represent three to five independent experiments. p values based on statistical analysis by one-way ANOVA with Dunnett's multiple comparison tests against tumor (**B**), unpaired Student's t-test (**E**) or paired Student's t-test (**C, F, G**), error bars indicate the SEM. (hu) indicates human samples. For measurements of protein translation rate presented throughout the manuscript, each T cell condition was treated ± CHX, and CHX-treated wells were used to normalize protein synthesis rates in various *in vivo* and *in vitro* conditions defined as $\log_2$ (T cell protein synthesis rate/T cell protein synthesis rate in the presence of CHX).

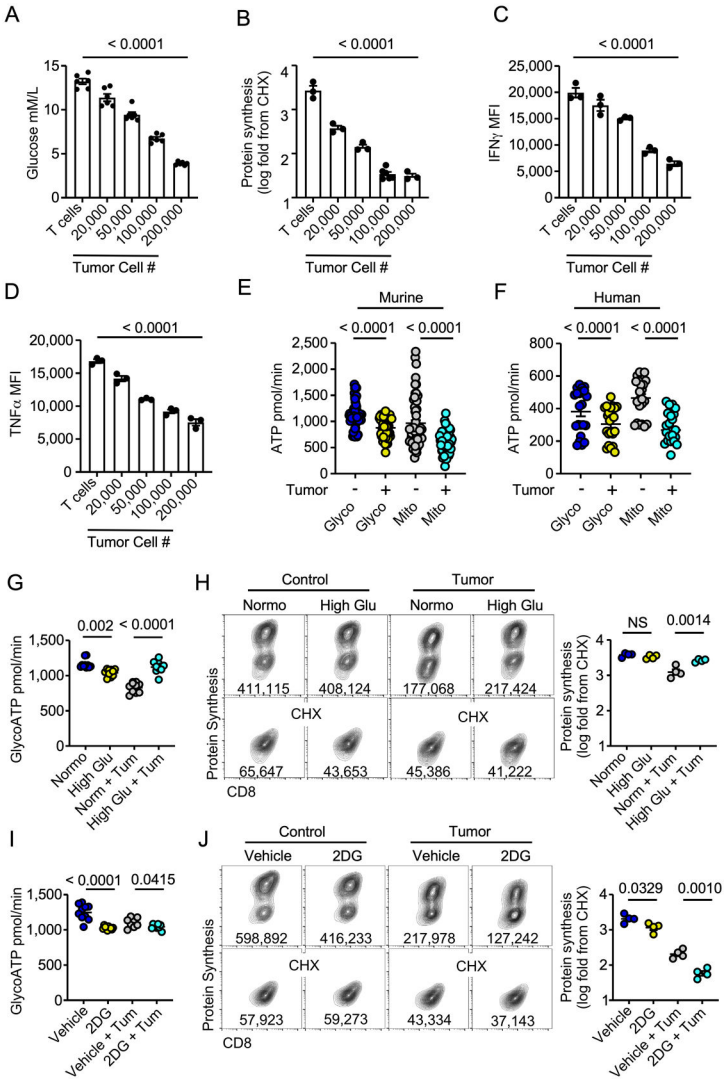

Figure 2. Glucose stress undermines T cell translation

Quantification of **A**) exogenous glucose concentration, **B**) protein synthesis rates, **C**) IFNγ or **D**) TNFα production from the tumor-T cell transwell assay with increasing numbers of tumor cells seeded prior to introduction of T cells **A-D**) Significance indicated in figure based on comparison between T cells vs T cells with 200,000 tumor cells. ATP rate measured by Seahorse Bioanalysis from glycolysis (glycoATP) or mitochondria (mitoATP) in **E**) OT-1 $CD8^+$ PBMC (n = 4 donors) in the tumor-T cell coculture transwell assay. Quantification of **G**) ATP rate from glycolysis or **H**) protein synthesis rate ± exogenous glucose (25mM) from OT-1 T cells in the tumor-T cell transwell assay. Quantification of **I**) ATP rate from glycolysis or **J**) protein synthesis rate with 2-deoxy-glucose (2DG) or vehicle added 2 hours prior to harvest to OT1 T cells in the tumor-T cell transwell assay. Glucose measurements, ATP rate data, and protein synthesis measurements represent one of three to six independent experiments. p values are noted based on statistical analysis by one-way ANOVA with a Dunnett's multiple comparison correction (**A-D**), one-way ANOVA with a

Tukey's multiple comparison correction (**E, G-J**), or paired Student's t-test (**F**), error bars indicate SEM.

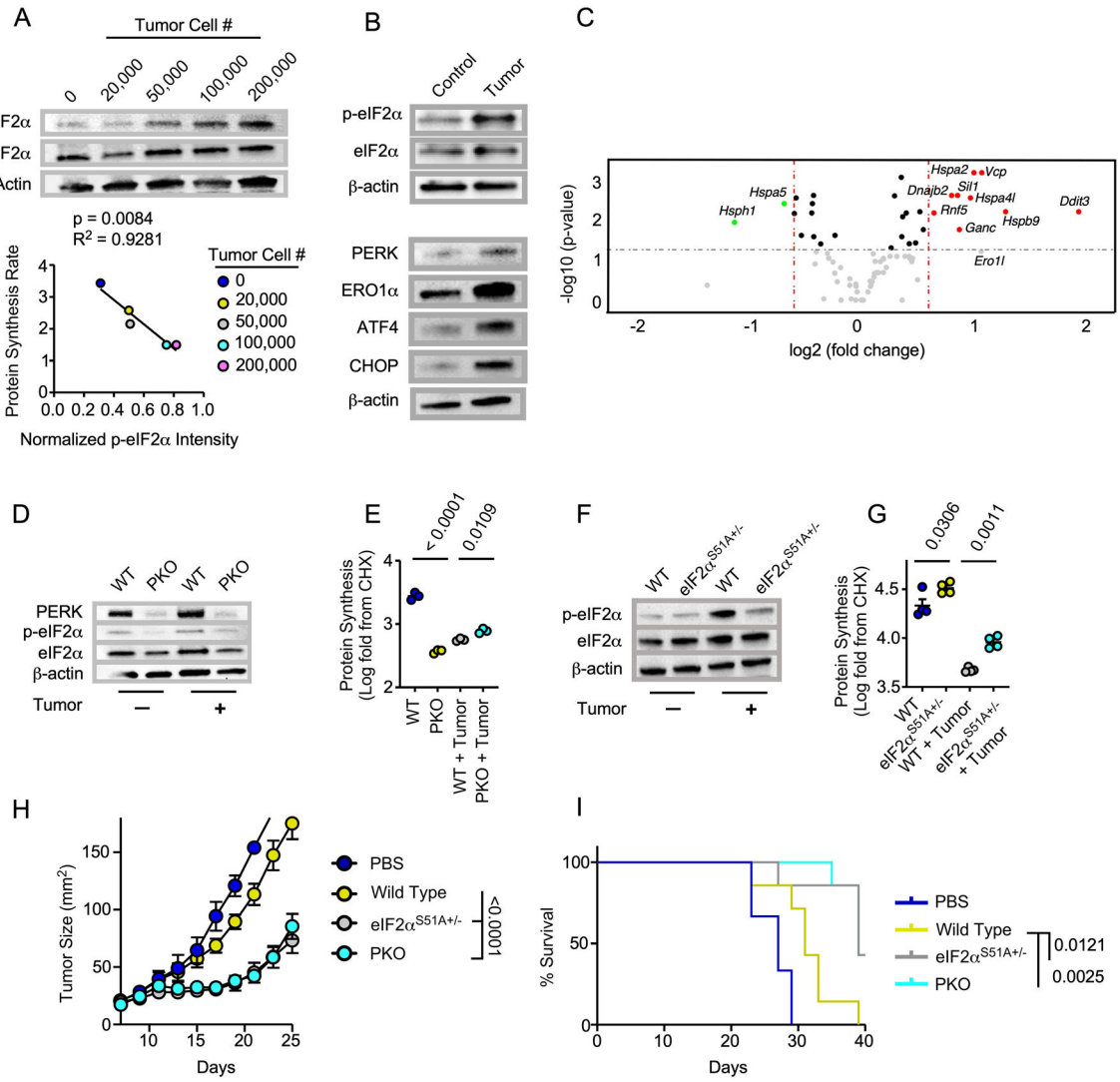

Figure 3. p-eIF2α attenuates T cell translation and tumor control

A) Western blot analysis from OT-1 T cells cocultured with ascending numbers of tumor cells in the tumor-T cell transwell coculture assay where normalized p-eIF2α intensities were correlated with protein synthesis rates **B**) Western bot analysis from OT-1 T cells harvested from the tumor-T cell transwell coculture assay. **C**) Volcano plot analysis from a targeted gene array measuring 83 common UPR associated genes from OT-1 T cells harvested from the tumor-T cell coculture assay. Genes in red are upregulated in tumor condition while genes in green are downregulated. **D, F**) Western blot analysis and **E, G)** quantification of protein synthesis murine or **F**) human rates from **D-E**) Lck*cre*PERK$^{f/f}$ (PKO) or wild type (WT) littermate OT-1 controls or **F-G)**, eIF2α$^{S51A+/-}$ or WT littermate OT-1 controls harvested from the tumor-T cell transwell assay. **H**) Tumor growth rate and **I**) overall survival from adoptive transfer of 7-day expanded PKO, eIF2α$^{S51A+/-}$, or WT littermate OT-1 T cells infused into CD57BL/6 mice bearing 7-day established B16-F1-OVA melanomas. For the experiment shown, eIF2α$^{S51A+/-}$ OT1 WT littermates were used. Western blot and FACS plots represent one of three to six independent experiments. UPR

gene array was performed with T cells from 3 control or tumor-seeded transwells. Tumor control experiments represent one of two independent experiments. p values are noted based on statistical analysis by linear regression (**A**), one-way ANOVA with Tukey's multiple comparison correction (**E,G**) mixed linear regression modeling (**H**) and log-rank, mantel-cox test of survival proportions (**I**), (N = 4-8 mice per group). Criteria for significance in the UPR gene array (**C**) were Fold Change > 1.5 and $p < 0.05$, normalization was performed using the ThermoFisher global normalization platform, all error bars indicate the SEM.

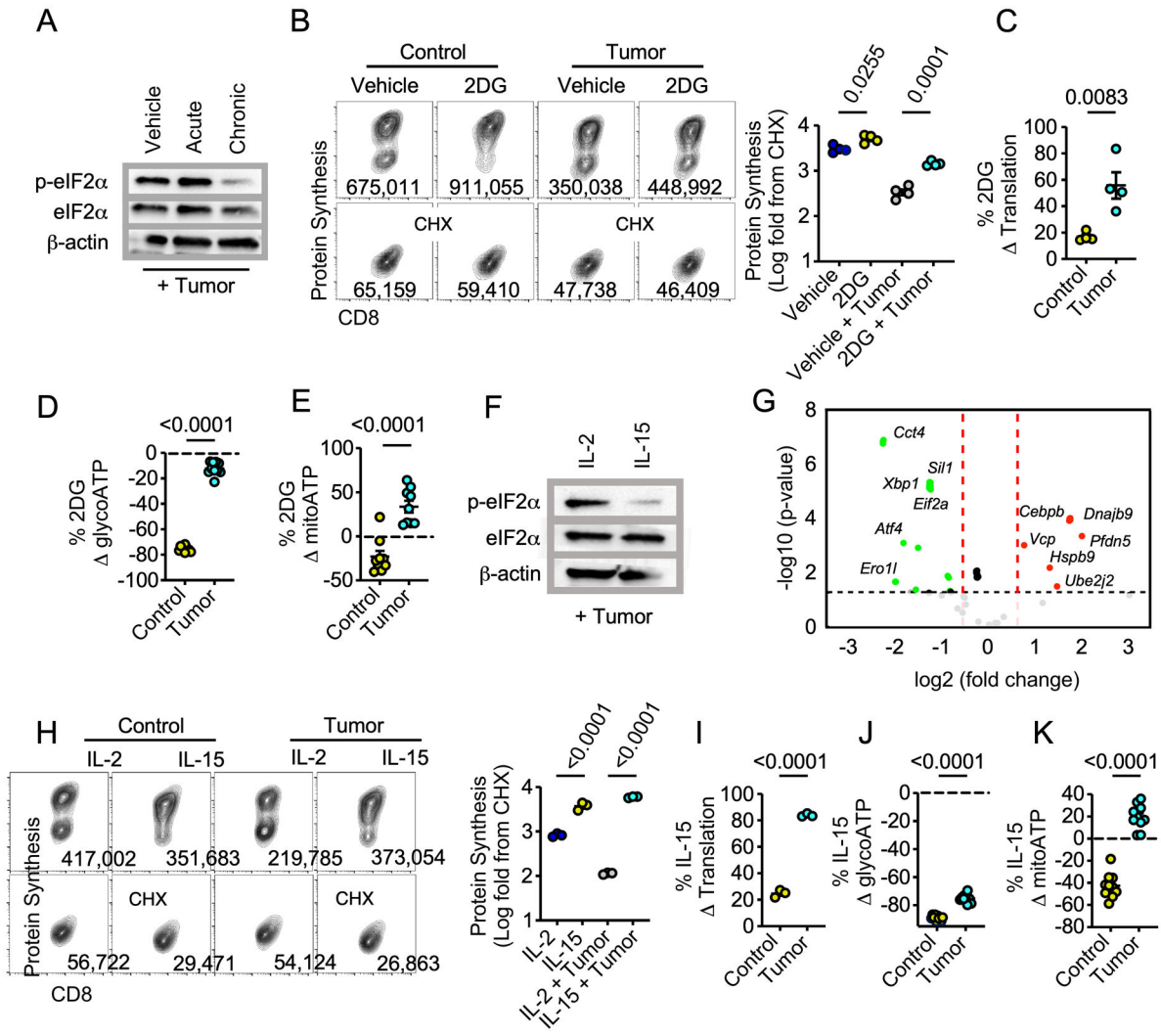

Figure 4. Metabolic reprogramming alleviates translation attenuation

A) Western blot analysis from OT-1 T cells cultured with vehicle, acute (2 hours), or chronic (36 hours) 2DG harvested from the tumor-T cells transwell coculture assay. **B**) Representative FACS plots and quantification of protein synthesis rates, and percent change in **C**) protein synthesis rate, **D**) glycolytic ATP or, **E**) mitochondrial ATP of chronic 2DG-treated OT1 T cells relative to vehicle controls from tumor or non-tumor conditions in the tumor-T cell transwell assay. **F**) Western blot analysis and **G**) Volcano plot analysis from a targeted gene array measuring 83 common UPR associated genes from OT-1 T cells conditioned with IL-2 or IL-15 prior to harvest from the tumor-T cell coculture assay. Genes in green are down regulated in the IL-15 condition relative to the IL-2 controls. **H**) Representative FACS plots and quantification of protein synthesis rates, and percent change in **I**) protein synthesis rate, **J**) glycolytic ATP or, **K**) mitochondrial ATP of IL-15 conditioned OT1 T cells relative to IL-2 controls from tumor or non-tumor conditions in the tumor-T cell transwell assay. Western blot and FACS plots represent one of three to six independent experiments. p values are noted in each panel based on statistical analysis by unpaired Student's t-test (**C-E, I-K**), one-way ANOVA with Tukey's multiple comparison

correction (**B, H**). Criteria for significance in the UPR gene array (**G**) were Fold Change > 1.5 and $p < 0.05$, normalization was performed using the ThermoFisher global normalization platform, all error bars indicate the SEM.

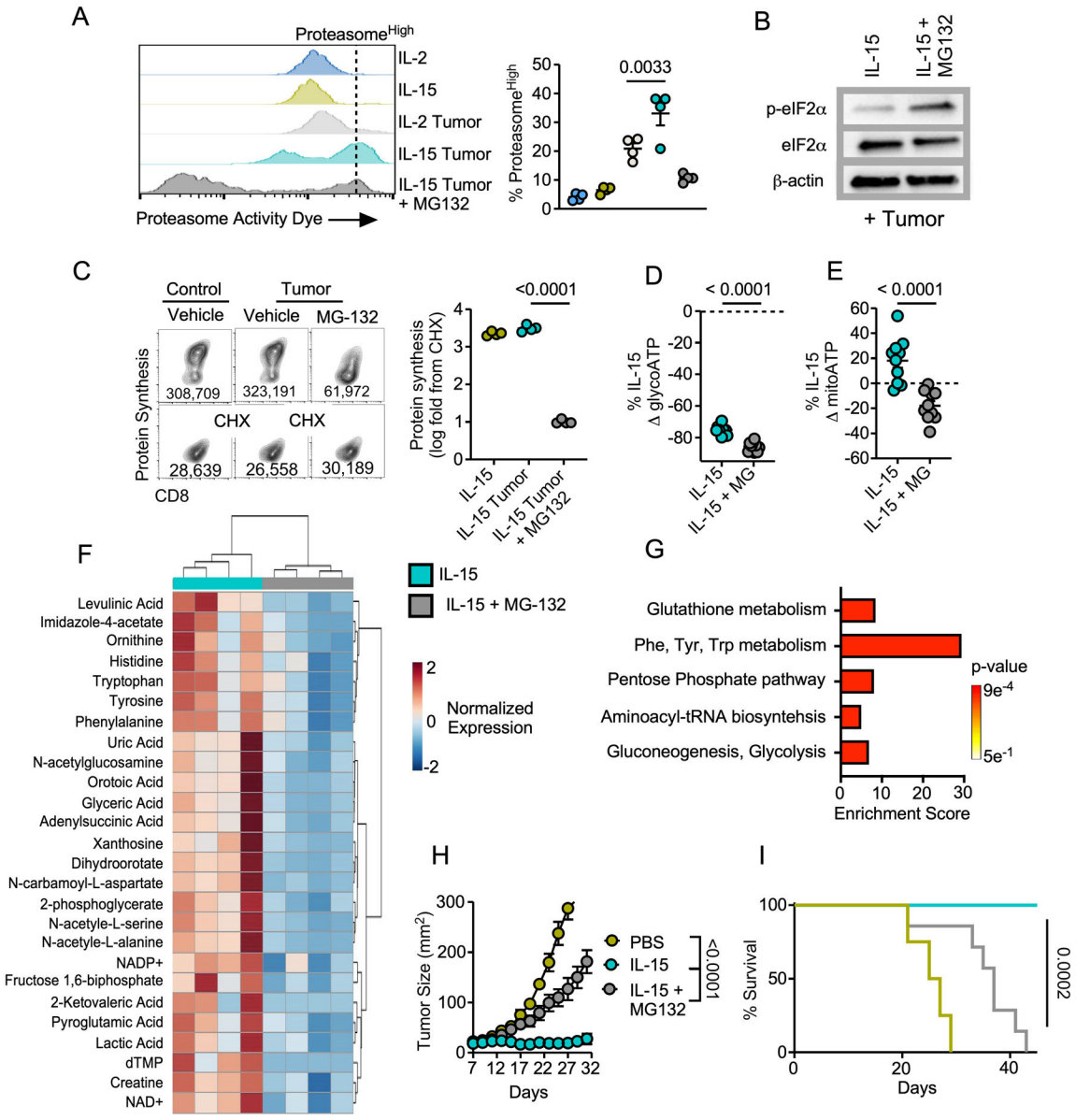

Figure 5. Proteasome function sustains translation and tumor immunity.

A) Representative histograms and quantification of the frequency of proteasome activity^{high} cells from IL-2 or IL-15 conditioned OT-1 T harvested from the tumor-T cell coculture assay. Proteasome inhibitor MG-132 was added as an internal control 2-4 hours prior to cell harvest. **B**) Western blot analysis, **C**) representative FACS plots and quantification of protein synthesis rates, and percent change in **D**) glycolytic ATP or **E)** mitochondrial ATP of IL-15 conditioned OT1 T cells treated with MG-132 or vehicle for 2-4 hours prior harvest from the tumor-T cell transwells. **F)** Heatmap of significantly enriched metabolites and **G**) pathway enrichment analysis in IL-15 conditioned OT-1 T cells treated with vehicle relative to MG-132 for 2-4 hours prior to harvest from the tumor-T cell transwell assay. **H**) Tumor growth rate and **I**) overall survival from adoptive transfer of 7-day expanded IL-15 conditioned OT-1 T cells treated with MG-132 or vehicle control for 4 hours prior to transfer

to B6 mice bearing 7-day established B16-F1-OVA melanomas. Data are representative of one to three independent experiments. p values are noted in each panel based on statistical analysis by one way ANOVA with Dunnett's (**A**) or Tukey's multiple comparison correction (**C**), unpaired Student's t-test (**D-E**) or mixed linear regression (**H**) and log-rank, mantel-cox test of survival proportions (**I**), (N = 4-8 mice per group), error bars indicate the SEM. Criteria for significant differences in metabolite fold change > 2 and raw p-value < 0.1 (**F, G**).

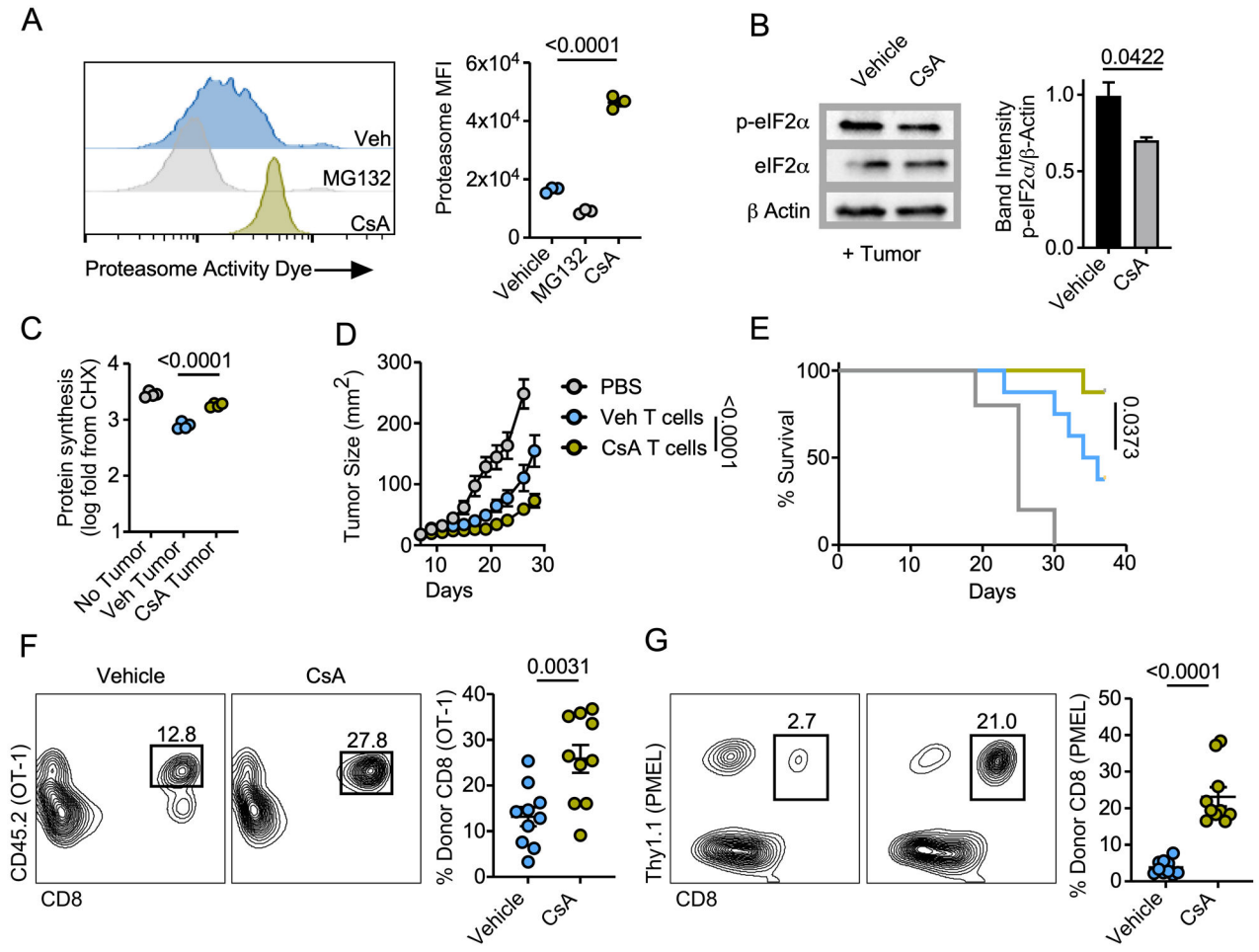

Figure 6. Proteasome stimulation enhances T cell tumor immunity

A) Proteasome activity of purified CD8$^+$ splenocytes treated for 4 hours with cyclosporine A (CsA) or MG-132. **B)** Western blot analysis and band quantification or **C**) quantification of protein synthesis rates from IL-2 effector T cells conditioned with CsA or vehicle control prior to seeding in the tumor-T cell transwell assay. **D**) Tumor growth rate and **E**) overall survival from adoptive transfer of 7-day expanded vehicle or CsA conditioned OT-1 T cells infused to C57BL/6 mice bearing 7-day established B16-F1-OVA melanomas. Frequency of adoptively transferred **F)** CD45.2$^+$ OT1 or **G)** Thy1.1$^+$ pmel T cells infused as in **D-E** harvested from B16-F1-OVA or B16-F1 melanomas 5 days post transfer, respectively. Data are representative of one to three independent experiments. p values are noted in each panel based on statistical analysis by one way ANOVA with Tukey's multiple comparison correction (**A, C**) two tailed Student's t-test (**B, F-G**) or mixed linear regression (**D**) and log-rank, mantel-cox test of survival proportions (**E**), (N = 4-8 mice per group), all error bars indicate the SEM.